# Neutron inclusive measurements of $^{36}Ar+Ag$ reactions at 35 MeV/nucleon

D. Sackett, A. Galonsky, C. K. Gelbke, H. Hama,* L. Heilbronn, D. Krofcheck,†
W. Lynch, H. R. Schelin,‡ M. B. Tsang, and X. Yang§
*National Superconducting Cyclotron Laboratory and Department of Physics and Astronomy, Michigan State University, East Lansing, Michigan 48824*

F. Deák, Á. Horváth, and Á. Kiss
*Department of Atomic Physics, Eötvös University, Budapest 114, Hungary H-1088*

Z. Seres
*Hungarian Academy of Sciences, Central Research Institute for Physics, Budapest 114, Hungary H-1525*

J. Kasagi
*Department of Physics, Tokyo Institute of Technology, O-Okayama, Meguro-Ku, Tokyo, Japan*

T. Murakami
*Department of Physics, Kyoto University, Kitasherakawa, Kyoto 606, Japan*
(Received 20 December 1990)

We have measured the inclusive neutron cross section as a function of neutron energy and angle at 15°, 30°, 45°, 60°, 120°, and 160° for the system Ag($^{36}$Ar,$n$) at 35 MeV/nucleon. All spectra can be fitted with a moving-source model consisting of a projectilelike source, an intermediate-rapidity source, and a targetlike source. Temperatures for the targetlike and intermediate-rapidity sources were found to be about 4 and 11 MeV, respectively. Neutron multiplicities for each were 5.6 and 1.0. These parameters are compared with those from the neutron inclusive measurement of Ag($^{14}$N,$n$) at 35 MeV/nucleon and with proton exclusive data from the reaction $^{32}S+Ag$ at 30 MeV/nucleon.

## I. INTRODUCTION

A good deal can be learned about heavy-ion reactions by examining the resulting neutron spectra. Sometimes, neutron yields are considered in coincidence with fragments, [1–5] but some gross features of the reaction mechanism, such as multiplicities and nuclear temperatures, can be deduced from inclusive experiments as well [6,7]. These measurements provide absolute cross sections for the energy and angle dependence of neutron production; thus comparison with theoretical calculations is easily achieved. Also, this type of measurement has other uses, for example, calibrating a $4\pi$ neutron ball. Although impact parameter selection is unavailable in an inclusive experiment, it will be shown that contributions from distinct sources can be unfolded from the neutron spectra using a standard moving-source model. It is our goal to gain some understanding of heavy-ion reactions by studying the pattern of neutron emission in different systems. As a beginning, we compare the resulting thermal fit parameters with those from the reaction Ag($^{14}$N,$n$) at 35 MeV/nucleon and with proton exclusive spectra from the $^{32}S+Ag$ reaction at 30 MeV/nucleon.

## II. EXPERIMENTAL PROCEDURE

Using a 35-MeV/nucleon $^{36}Ar^{11+}$ beam provided by the K500 Cyclotron at Michigan State University (MSU), we have measured inclusive neutron spectra from the reaction Ag($^{36}$Ar,$n$) at angles of 15°, 30°, 45°, 60°, 120°, and 160°. The target consisted 2.57 mg/cm$^2$ of natural silver and was rotated such that its normal made an angle of 60° with respect to the beam direction. The detectors and measurement technique are described in detail in Ref. [7]. Figure 1 shows the experimental setup. Detectors on the left side of the beam (positive angles) were positioned with flight paths ranging from 160 to 250 cm. To achieve better energy resolution when detecting higher-energy neutrons, detectors on the right side of the beam (negative angles) were placed at distances ranging from 350 to 450 cm. For these flight paths, several detectors were bundled together to provide a counting rate similar to that of the detectors at positive angles. The rectangular boxes represent cylindrical brass or steel bars (shadow bars) ranging from 20 to 30 cm in length. Data collected without the bars include neutrons coming directly to a detector from the target and neutrons scattered into a detector from the scattering chamber or other areas of the vault. Data collected with the bars shadowing the detector from the target comprise all the background neutrons. Subtracting these spectra then gives only the neutron yields from the target. In this experiment all the shadow bars were put in place for the background measurement. The question arises as to whether the bars distort the neutron background by providing additional scattering material not present during the nonshadow bar measurements. In the first such neutron experiment [4]

 

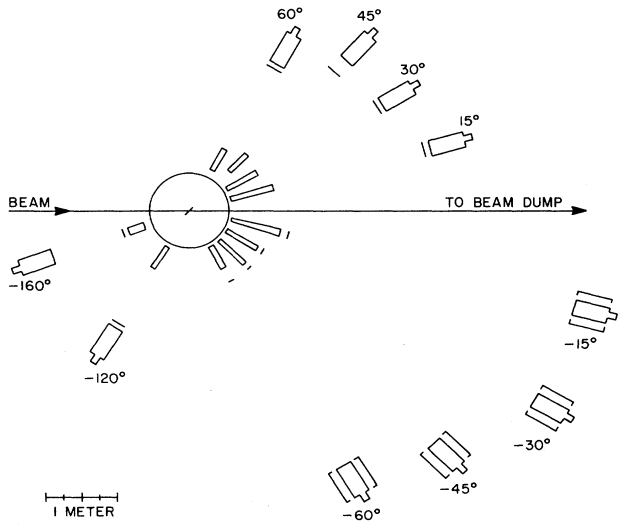


FIG. 1. Experimental setup. Groups of detectors were placed at the angles −15°, −30°, −45°, and −60° and are enclosed in brackets. Single detectors were placed at +15°, +30°, +45°, +60°, −120°, and −160°. The flight paths ranged from 160 to 450 cm. The rectangular boxes represent shadow bars (the −15° bar is tapered), and the solid lines in front of detectors or behind shadow bars represent the proton veto paddles.

at MSU, this effect was investigated. The neutron background was determined once with only alternate bars in place and once with all of the bars in place. No difference, within statistical uncertainties, was found between the two measurements. The small lines in front of the detectors or shadow bars represent veto paddles. They are thin plastic scintillators that are used to reject high-energy protons and deuterons that enter the neutron detectors. All charged particles with $Z \geq 2$ are stopped in the material between the target and detectors.

The timing was performed as follows: An event in a detector served as a start signal for a time-to-digital converter (TDC). The cyclotron period was ~52 ns, and so a TDC stop signal from the cyclotron rf, scaled by a factor of 2, came approximately every 104 ns. Half of a typical time-of-flight spectrum is shown in Fig. 2 (the other half would be a similar spectrum between channels 175 and 275). Shown are both the total neutron spectrum (including background) and the background contribution. Also shown is the location of the gamma-ray peak. From the location of the gamma-ray peak in the time-of-flight spectrum and a calibration (ns/channel) of the TDC, the time of flight of a neutron can be calculated directly. Neutrons were distinguished from gamma rays using pulse-shape discrimination [8]. Neutron detector efficiencies, typically between 10% and 20%, were calculated from a Monte Carlo code [9]. The uncertainty in

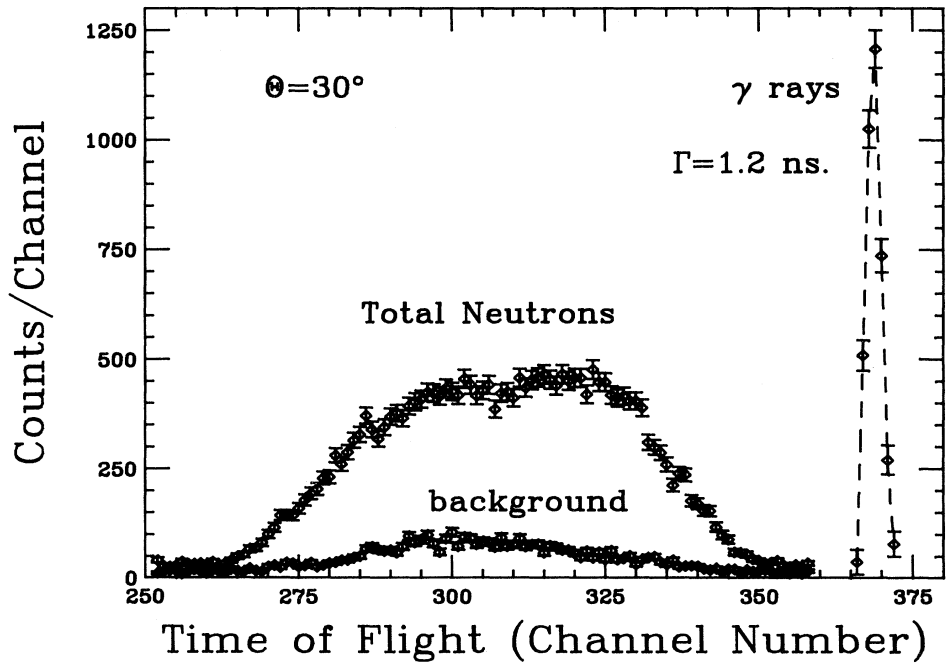


FIG. 2. Typical time-of-flight spectrum for neutrons and $\gamma$ rays. The data for total neutrons includes target and background contributions. The background contribution is also shown separately. Subtracting the background from the total gives the target neutron. The width of the $\gamma$ peak is 1.2 ns. The time-to-digital converter calibration is 0.2607 ns/channel.

the efficiencies is 10% [9].

The neutron yields are binned as counts per time bin versus time of flight. Converting the time-of-flight bin to an energy bin gives the neutron yield in counts per MeV vs energy. The neutron yields are attenuated when passing through the steel scattering chamber and, for some angles, up to 10 mm of silicon (due to the fragment telescopes). Where no silicon is present, typical attenuations are 13% for 25-MeV neutrons and 8% for 75-MeV neutrons. When the flight path contained the silicon telescopes, attenuations for 25-MeV neutrons were about 25% and for 75-MeV neutrons about 18%. Folding in the detector efficiency and the percentage of attenuations gives the final neutron energy spectrum.

Because the cyclotron period is only 52 ns, the low-energy spectrum is contaminated by high-energy neutrons from a subsequent beam pulse. To obtain the low-energy neutron spectrum, the high-energy contribution was subtracted using the following technique: Setting a high pulse-height threshold for the detector provides the high-energy spectrum with no overlapping low-energy contribution. At a low threshold, this spectrum changes only by the ratio of detection efficiencies for the high and low thresholds; hence the high-energy neutron spectrum at low pulse-height thresholds can be obtained. This scaled high-energy spectrum is then subtracted from a neutron spectrum obtained at a low threshold, thus leaving an uncontaminated low-energy spectrum. For detectors at positive angles, low-energy thresholds of 4.0–6.0 MeV (neutron energy) were used.

## III. RESULTS AND DISCUSSION

Figure 3 shows the double-differential neutron cross-section data. It is the behavior of the energy spectra that justifies a moving source analysis. At 45° and 60°, the spectra appear to be superpositions of two distinct components which vary exponentially with energy. In terms of a nuclear temperature, the low-energy neutron data possess a steeper slope, therefore indicating a cooler source. The higher-energy neutrons stem from a hotter source, because the slope of the data is much flatter. The spectra at 120° and 160° decrease exponentially with increasing energy. Because the data at 120° and 160° have such similar magnitudes, it can be inferred that the source is moving slowly enough to provide nearly isotropic emission. The enhancement in the 15° spectrum arises from rapidly moving sources created by peripheral collisions, and so their contribution appears only at forward angles. To proceed with the fitting, it is assumed that the sources are Maxwellian in nature and emit neutrons isotropically in their own rest frames. Assuming volume emission, the neutron distribution in a source rest frame is

$$\frac{d^2\sigma_n}{dE'd\Omega'} = \frac{N\sqrt{E'/\pi}}{2\pi T^{3/2}} \exp\left[\frac{-E'}{T}\right] .$$

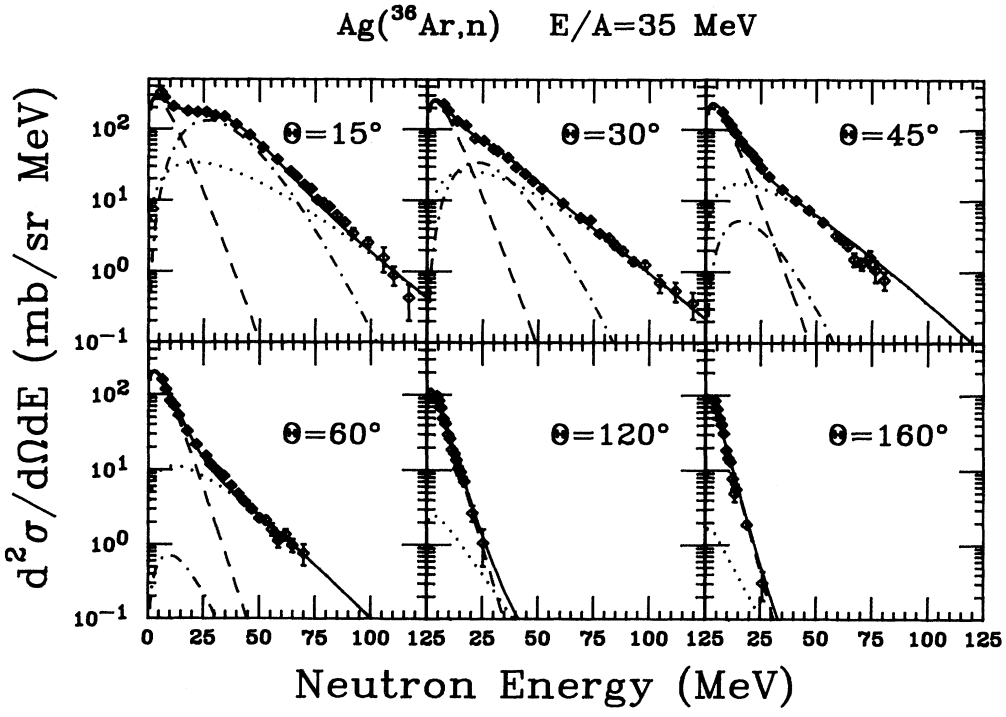


FIG. 3. (a)–(f) Neutron energy spectra at six angles. The solid lines are the fits using three thermal sources. The dot-dashed line is the contribution from the projectilelike source, the dotted line that of the intermediate-rapidity source, and the dashed line is the contribution of the targetlike source.

TABLE I. Temperatures, source velocities, source strengths, and multiplicities for a three-source fit to the neutron spectra for the reaction $^{36}$Ar(Ag,$n$). The data of Schelin *et al.* [7] is in parenthesis and that of Wada *et al.* [15] is in brackets. Missing uncertainties denote a fixed parameter in the fitting procedure. The final column is the total kinetic energy of the neutrons from the $i$th source.

| Source | $T$ (MeV) | $\epsilon$ (MeV/nucleon) | $N$ (b) | Multiplicity | $E_n'$ (MeV) |
|---|---|---|---|---|---|
| TLS | 4.2±0.3 | 0.56±0.13 | 19.1±1.7 | 5.6±0.7 | 35±7 |
| | (4.0±0.2) | (0.45±0.02) | (12.2±1.1) | (4.5±0.6) | (27±6) |
| | [5.4±0.4] | [0.83] | | [2.4±0.2] | |
| IRS | 11.4±1.3 | 11.77±2.0 | 3.9±0.5 | 1.1±0.2 | 20±6 |
| | (11.1±0.6) | (12.8±0.5) | (2.32±0.2) | (0.86±0.11) | (14±3) |
| | [11.0±1.2] | [14.3±1.9] | | [1.5±0.2] | |
| PLS | 3.6±0.4 | 24.6±1.8 | 3.2±0.4 | 0.9±0.1 | 5±1 |
| | (2.2±0.3) | (30.1±3.6) | (0.71±0.06) | (0.26±0.04) | (1±0.3) |
| | [4.0±0.7] | [28.0] | | [0.15±0.06] | |
| Totals | | | | 7.6±0.7 | 60±9 |
| | | | | (5.6±0.7) | (42±7) |

Here $E'$ is the neutron energy in the source rest frame, $\Omega'$ is the solid angle in the source rest frame, $T$ is the temperature in MeV, and $N$ is the neutron production cross section in barns. $E'$ is related to the laboratory neutron energy $E$ by

$$E'=E+\epsilon-2\sqrt{\epsilon E}\cos\theta ,$$

where $\epsilon$ is the kinetic energy per nucleon of the source and $\theta$ is the laboratory scattering angle. Summing over three sources, the parametrization in the laboratory frame of reference takes the following form:

$$\frac{d^2\sigma_n}{dE\,d\Omega}=\sum_{i=1}^{3}\frac{N_i\sqrt{E/\pi}}{2\pi T_i^{3/2}} \times\exp\left[-\left[\frac{E-2\sqrt{\epsilon_i E}\cos\theta+\epsilon_i}{T_i}\right]\right] .$$

The nine fit parameters are $N$, $T$, and $\epsilon$ for each source. The fitting was performed using a $\chi^2$ minimization procedure. The $\chi^2$ per degree of freedom was 3.71. Uncertainties correspond to the change in a parameter that increases $\chi^2$ by 1, with all other parameters fixed at their optimum values [10].

Table I summarizes the best-fit values of the parameters, and Fig. 3 displays the data and the overall fit. The values of the fit parameters confirm the characteristics attributed to each source. Thus the moving-source analysis, while providing a good fit to the data, also contains a reasonable description of the reaction dynamics. For example, there is a slowly moving targetlike source (TLS) that deexcites via neutron and charged-particle evaporation, and a hotter ($T\approx 11$ MeV) intermediate-rapidity source (IRS) moving with $V\approx V_{\rm beam}/2$ that deexcites in a similar manner. Finally, there is a projectilelike source (PLS) moving with a speed close to the beam velocity. Because the PLS originates from peripheral collisions, it must be noted that the assumption of thermal equilibrium, although convenient, is an oversimplification [11]. This source is included in the parametrization because it provides a useful fit to the spectra at the most forward angles. The remaining parameter, the neutron cross section $N_i$, is related to the multiplicity of the $i$th source as $M_i=N_i/\sigma_{\rm tot}$. The total reaction cross section is calculated from

$$\sigma_{\rm tot}=\pi[r_0(36^{1/3}+108^{1/3})]^2=3.40\ \text{b}$$

with $r_0=1.29$ fm [7]. A 10% error is assumed in $\sigma_{\rm tot}$ [7]. The calculated neutron multiplicities are also shown in Table I. The multiplicities are also meaningful in terms of the moving-source analysis. The low-energy part of the spectrum is well described by a purely exponential function of energy and is attributed to a targetlike remnant that deexcites via neutron and charged-particle evaporation. Coincidence measurements of neutrons and intermediate-mass fragments ($3\le Z\le 5$) [5] or neutrons and fission fragments [12] for systems with similar targets and beam energies find TLS multiplicities between 5 and 7, in agreement with our result of 5.6. The intermediate-rapidity source models the early stage of the reaction, where nucleon-nucleon collisions largely determine the spectrum. For beam energies around 30–35 MeV/nucleon, neutron multiplicities ranging from one to three have been found [5,13], again in agreement with our value of 1.1.

## IV. COMPARISON WITH OTHER EXPERIMENTS

The most direct comparison can be made with the data of Schelin *et al.* [7]. They have measured inclusive neutron spectra for $^{14}$N on Ag at 35 MeV per nucleon. Table I compares their moving-source parameters (in parenthesis) to ours. The final column in Table I represents the kinetic energy of the neutrons from the $i$th source, evaluated in the center-of-mass system. This kinetic energy is calculated from

$$E_{n_i}'=\int_0^\infty\frac{dN_i(E')}{dE'}E'dE' .$$

$dN_i/dE'$, the number of neutron/MeV from the $i$th source, is

$$\frac{dN_i}{dE'} = \frac{1}{\sigma_{\text{tot}}} \left[ \frac{d\sigma_n}{dE'} \right]_i ,$$

where $\sigma_{\text{tot}}$ is the total reaction cross section defined previously. Explicitly, the integral appears as

$$E'_{n_i} = \frac{2N_i}{\sqrt{\pi}\sigma_{\text{tot}} T_i^{3/2}} \int_0^\infty E'^{3/2} e^{-E'/T_i} dE' = \tfrac{3}{2} M_i T_i .$$

### A. Targetlike source

For the targetlike source, the multiplicities and temperatures are approximately the same for both systems. Since the temperature of the source is directly related to its excitation energy, this is a surprising result when the available energy in the center-of-mass reference frame ($E'_{\text{c.m.}}$) is considered. For the nitrogen projectile, $E'_{\text{c.m.}}$ is 434 MeV, and for the argon beam, $E'_{\text{c.m.}}$ is 945 MeV, an increase by a factor of 2.2. It would seem that a large increasing excitation energy would create a more highly excited TLS, thus causing significant changes in the temperature and multiplicity parameters. The data imply that this is not happening. The source multiplicities and temperatures (and therefore excitation energies) are essentially the same for each projectile. Also, the total kinetic energy of the emitted neutrons (final column Table I) only changes from 27 MeV (nitrogen beam) to 35 MeV for the argon beam, an increase of about 30%. One possible explanation is that, for either projectile, the TLS evaporates its lightly bound neutrons, but as it becomes more neutron deficient, separation energies increase such as to suppress further emission. Another factor is that with a larger projectile (argon) the geometric probability of incomplete fusion versus complete fusion is greater. By incomplete fusion we mean any collision where a significant projectilelike spectator is formed. Of course, at higher excitation energies, new fragmentation decay channels may become available such that neutron evaporation is deemphasized. In fact, fragment multiplicities ($M_{\text{frag}}$) for both projectiles on a silver target have recently been measured [14]. For the nitrogen projectile, $M_{\text{frag}}=0.06$, while for the argon beam, $M_{\text{frag}}=0.33$, an increase by a factor of 5.5.

It is also interesting to compare proton spectra from a similar reaction. Wada *et al.* [15] have determined temperatures, multiplicities, and source velocities in a similar three-source model for light charged particles ($Z \leq 2$) in coincidence with heavy residues and fragments for a 30-MeV/nucleon $^{32}$S beam on a silver target. Individual sets of parameters are given for reactions based on 40%, 60%, 80%, and 100% of the full momentum transfer between projectile and target. This is essentially an indication of the impact parameter of the reaction, since a large percentage of projectile momentum transferred to the target implies a more central collision. Because an inclusive experiment measures yields without regard to the centrality of the collision, it seems appropriate to average the parameters for the proton data over the percentages of full momentum transfer before comparing to our neutron inclusive results. The results appear in brackets in Table I. The source velocities in the data of Wada *et al.* are given as the ratio of source velocity to beam velocity ($\beta_s/\beta_{\text{inc}}$). These can be transformed to the source kinetic energy per nucleon ($\epsilon_i$). The compound nucleus source in their work is equated to our targetlike source. The multiplicities for the TLS are lower, but this can be attributed to the Coulomb barrier that restricts low-energy proton emission. The remaining parameters are in reasonable agreement.

### B. Intermediate-rapidity source

The IRS describes the contribution to the neutron spectra from the early part of the interaction between projectile and target, where individual nucleon-nucleon collisions are important. In this regime the velocity of the projectile nucleons is a major factor in determining the resulting neutron kinetic-energy spectra. For the experiments with argon and nitrogen projectiles, the nucleon velocities are identical, and so similar kinetic-energy spectra are expected. Because the source temperature reflects the resulting kinetic-energy spectra, the temperatures should therefore be similar. From Table I, this is certainly the case. For argon and nitrogen projectiles, the IRS temperatures are 11.4 and 11.1 MeV, respectively. Because the argon projectile is more massive and therefore contributes more kinetic energy to the target, the energy will be dissipated over a larger region of the target. Thus the source size is expected to increase, but not the temperature. It is also interesting that the IRS temperature for the proton exclusive data of Wada *et al.* ($T=11.0$ MeV) is in agreement with the neutron inclusive source temperatures.

Again referring to Table I, we find that there is only a small increase in the IRS multiplicity (from 0.86 to 1.1) for the Ag($^{36}$Ar,$n$) reaction, compared to the Ag($^{14}$N,$n$) reaction. This is a surprising result, considering that IRS neutron spectra are largely determined by nucleon-nucleon collisions and that there are $\sim$2.6 times as many nucleons in the argon projectile. Possibly the same effects that suppress the TLS multiplicity exist here also. Referring to the data of Hama *et al.* [14], the fragment multiplicities for the nitrogen and argon beams are 0.08 and 0.38, respectively, an increase by about a factor of 5. The IRS proton multiplicity of Wada *et al.* is similar to the neutron multiplicity with the argon projectile. Unlike the TLS, which describes predominantly low-energy spectra, the IRS is responsible for the high-energy part of the spectra, and so Coulomb barrier effects are no longer significant.

### C. Projectilelike source

Since the main difference between the Ar+Ag and N+Ag systems is the size of the projectile, it should not be surprising that the fit parameters for the PLS are affected the most. The multiplicity for the argon projectile is $\sim$3 times greater, which should be expected since there are $\sim$2.6 times as many neutrons in the argon projectile. Also, the temperature and the total neutron ki-

netic energy ($E_n'$) are higher, whereas the source velocity is a bit lower. This implies a greater exchange of energy and momentum between target and projectile for grazing collisions. The PLS parameters of Wada *et al.* are also listed in Table I. The values for temperature and kinetic energy per nucleon are in agreement with the Ar+Ag fit parameters, although the multiplicity is significantly different. Again, Coulomb barrier effects may be affecting proton emission. However, it must be reemphasized that treating the PLS as a thermal source is an oversimplification [11]; hence comparison of thermal fit parameters should not be taken too literally.

## V. CONCLUSIONS

We have measured the inclusive neutron spectra for the reaction Ag($^{36}$Ar,$n$) at 35 MeV/nucleon. The energy spectrum at several angles can be fitted with three moving sources, and the resulting fit parameters are physically reasonable. Comparing our temperatures, multiplicities, and total neutron kinetic energies to values found in previous lower-energy work, we find that a large increase in available excitation energy does not manifest itself in more highly excited sources and higher neutron multiplicities. One possible explanation is that there may be alternative modes of deexcitation at higher energies. Further studies measuring both inclusive and exclusive neutron spectra over ranges of bombarding energies, with the same target and projectile, would provide the systematics to study this interesting effect.

## ACKNOWLEDGMENTS

Support of the U.S. National Science Foundation under Grants No. Int-86-17683 and No. Phy-86-11210 and of the Hungarian Academy of Sciences is gratefully acknowledged.

*Permanent address: Ultraviolet Synchrotron Orbital Radiation Laboratory, Institute for Molecular Science, Myodaiji, Okazaki 444, Japan.

†Current address: Lawrence Livermore National Laboratory, Livermore, CA 94550.

‡Permanent address: Centro Tecnico Aeroespacial and supported in part by CNPq, Brazil.

§Current address: Ohio University, Athens, OH 45701.

[1] D. Hilscher, J.R. Birkelund, A. D. Hoover, W. U. Schröder, W. W. Wilcke, J. R. Huizenga, A. C. Mignerey, K. L. Wolf, H. F. Breuer, and V. E. Viola, Phys. Rev. C **20**, 576 (1979).

[2] Y. Eyal, A. Gavron, I. Tserruya, Z. Fraenkel, Y. Eisen, S. Wald, R. Bass, G. R. Gould, G. Kreyling, R. Renfordt, K. Stelzer, R. Zitzmann, A. Gobbi, U. Lynen, H. Stelzer, I. Rode, and R. Bock, Phys. Rev. Lett. **41**, 625 (1978).

[3] A. Galonsky, G. Caskey, L. Heilbronn, B. Remington, H. Schelin, F. Deak, Á. Kiss, Z. Seres, and J. Kasagi, Phys. Lett. B **197**, 511 (1987).

[4] F. Deak, Á. Kiss, Z. Seres, G. Caskey, A. Galonsky, C. K. Gelbke, B. Remington, M. B. Tsang, and J. J. Kolata, Nucl. Phys. **A464**, 133 (1987).

[5] C. Bloch, W. Benenson, A. Galonsky, E. Kashy, J. Heltsley, L. Heilbronn, M. Lowe, R. J. Radtke, B. R. Remington, J. Kasagi, and D. J. Morrissey, Phys. Rev. C **37**, 2469 (1988).

[6] D. Fox, D. A. Cebra, J. Karn, C. Parks, G. D. Westfall, and W. K. Wilson, Phys. Rev. C **36**, 640 (1987).

[7] H. R. Schelin, A. Galonsky, C. K. Gelbke, L. Heilbronn, W. G. Lynch, T. Murakami, M. B. Tsang, X. Yang, G. Zhang, B. A. Remington, F. Deak, Á. Kiss, Z. Seres, and J. Kasagi, Phys. Rev. C **39**, 1827 (1989).

[8] J. Heltsley, L. Brandon, A. Galonsky, L. Heilbronn, B. A. Remington, S. Langer, A. VanderMolen, and J. Yurkon, Nucl. Instrum. Methods Phys. Res. A **263**, 441 (1988).

[9] R. A. Cecil, B. D. Anderson, and R. Madey, Nucl. Instrum. Methods **161**, 439 (1979).

[10] P. R. Bevington, program CURFIT, in *Data Reduction and Error Analysis for the Physical Sciences* (McGraw-Hill, New York, 1969), p. 237.

[11] Á. Kiss, F. Deak, Z. Seres, G. Caskey, A. Galonsky, L. Heilbronn, B. A. Remington, and J. Kasagi, Phys. Lett. B **184**, 149 (1987).

[12] J. Galin, Nucl. Phys. **A488**, 297 (1988).

[13] D. Hilscher, H. Rossner, A. Gamp, U. Jahnke, B. Cheynis, B. Chambon, D. Drain, C. Pastor, A. Giorni, C. Morand, A. Dauchy, P. Stassi, and G. Petitt, Phys. Rev. C **36**, 208 (1987).

[14] H. Hama *et al.* (unpublished).

[15] R. Wada, D. Fabris, K. Hagel, G. Nebbia, Y. Lou, M. Gonin, J. B. Natowitz, R. Billerey, B. Cheynis, A. Demeyer, D. Drain, D. Guinte, C. Pastor, L. Vagneron, K. Zaid, J. Alarja, A. Giorni, D. Heuer, C. Morand, B. Viano, C. Mazur, C. Ngô, S. Leray, R. Lucas, M. Ribrag, and E. Tomasi, Phys. Rev. C **39**, 497 (1989).